ARTICLE IN PRESS

Deep-Sea Research II ▮ (▮▮▮▮) ▮▮▮–▮▮▮

Contents lists available at SciVerse ScienceDirect

Deep-Sea Research II

journal homepage: www.elsevier.com/locate/dsr2

Change in El Niño flavours over 1958–2008: Implications for the long-term trend of the upwelling off Peru

B. Dewitte [a,*], J. Vazquez-Cuervo [b], K. Goubanova [c,a], S. Illig [a,d], K. Takahashi [e], G. Cambon [a], S. Purca [d], D. Correa [f], D. Gutierrez [d,g], A. Sifeddine [h,i], L. Ortlieb [h]

[a] LEGOS/IRD, Toulouse, France
[b] JPL/Caltech/NASA, Pasadena, USA
[c] CNES, Toulouse, France
[d] Instituto del Mar del Peru, Callao, Peru
[e] Instituto Geofisico del Peru, Lima, Peru
[f] Servicio Nacional de Meteorología e Hidrología del Perú, Lima, Peru
[g] Programa Maestria en Ciencias del Mar, Universidad Peruana Cayetano Heredia, Lima, Peru
[h] LOCEAN/IRD, Paris & Bondy, France
[i] LMI PALEOTRACES, Departamento de Geoquimica, Universidade Federal Fluminense, Niteroi, Brasil

ARTICLE INFO

Keywords:
El Niño Modoki
Equatorial Kelvin wave
Climate change
Coastal upwelling
Peru undercurrent

ABSTRACT

The tropical Pacific variability has experienced changes in its characteristics over the last decades. In particular, there is some evidence of an increased occurrence of El Niño events in the central Pacific (a.k.a. 'Central Pacific El Niño' (CP El Niño) or 'El Niño Modoki'), in contrast with the cold tongue or Eastern Pacific (EP) El Niño which develops in the eastern Pacific. Here we show that the different flavours of El Niño imply a contrasted Equatorial Kelvin Wave (EKW) characteristic and that their rectification on the mean upwelling condition off Peru through oceanic teleconnection is changed when the CP El Niño frequency of occurrence increases. The Simple Ocean Data Assimilation (SODA) reanalysis product is first used to document the seasonal evolution of the EKW during CP and EP El Niño. It is shown that the strong positive asymmetry of ENSO (El Niño Southern Oscillation) is mostly reflected into the EKW activity of the EP El Niño whereas during CP El Niño, the EKW is negatively skewed in the eastern Pacific. Along with slightly cooler conditions off Peru (shallow thermocline) during CP El Niño, this is favourable for the accumulation of cooler SST anomalies along the coast by the remotely forced coastal Kelvin wave. Such a process is observed in a high-resolution regional model of the Humboldt Current system using the SODA outputs as boundary conditions. In particular the model simulates a cooling trend of the SST off Peru although the wind stress forcing has no trend. The model is further used to document the vertical structure along the coast during the two types of El Niño. It is suggested that the increased occurrence of the CP El Niño may also lead to a reduction of mesoscale activity off Peru.

© 2012 Elsevier Ltd. All rights reserved.

1. Introduction

Many recent studies have reported the existence of more than one type of El Niño (or warm El Niño Southern Oscillation (ENSO) event) based on spatial distributions of Sea Surface Temperature (SST) (Ashok et al., 2007; Kao and Yu, 2009; Kug et al., 2009; Larkin and Harrison, 2005; Weng et al., 2007; Yeh et al., 2009). So far, the ENSO has been categorised into two types of El Niño: (1) the traditional Cold Tongue El Niño or Eastern Pacific El Niño (hereafter EP El Niño) that consists of the SST anomaly developing and peaking in the eastern equatorial Pacific and (2) the so-called Modoki El Niño (Ashok et al., 2007) or Central Pacific El Niño (Kao and Yu, 2009; hereafter CP El Niño) that consists of the SST anomaly developing and persisting in the central Pacific. Whereas the dynamics of the EP El Niño has been well documented (McPhaden et al., 1998), the observed increased occurrence of the CP El Niño during the last decades (Lee and McPhaden, 2010; Takahashi et al., 2011; Yeh et al., 2009) has led the community to investigate the mechanisms responsible for the triggering, development and decay of this different flavour of El Niño (Kug et al., 2009; Yu and Kim, 2010, 2011; Yu et al., 2010). The CP El Niño implies a significantly different zonal SST gradient across the entire equatorial Pacific than during the EP El Niño and therefore a contrasted ENSO atmospheric teleconnection (Ashok et al., 2007; Weng et al., 2009; Yeh et al., 2009). Fig. 1 (top) shows the El Niño

* Corresponding author.
E-mail address: bxd@legos.obs-mip.fr (B. Dewitte).

0967-0645/$ - see front matter © 2012 Elsevier Ltd. All rights reserved.
http://dx.doi.org/10.1016/j.dsr2.2012.04.011

Please cite this article as: Dewitte, B., et al., Change in El Niño flavours over 1958–2008: Implications for the long-term trend of the upwelling off Peru. Deep-Sea Res. II (2012), http://dx.doi.org/10.1016/j.dsr2.2012.04.011

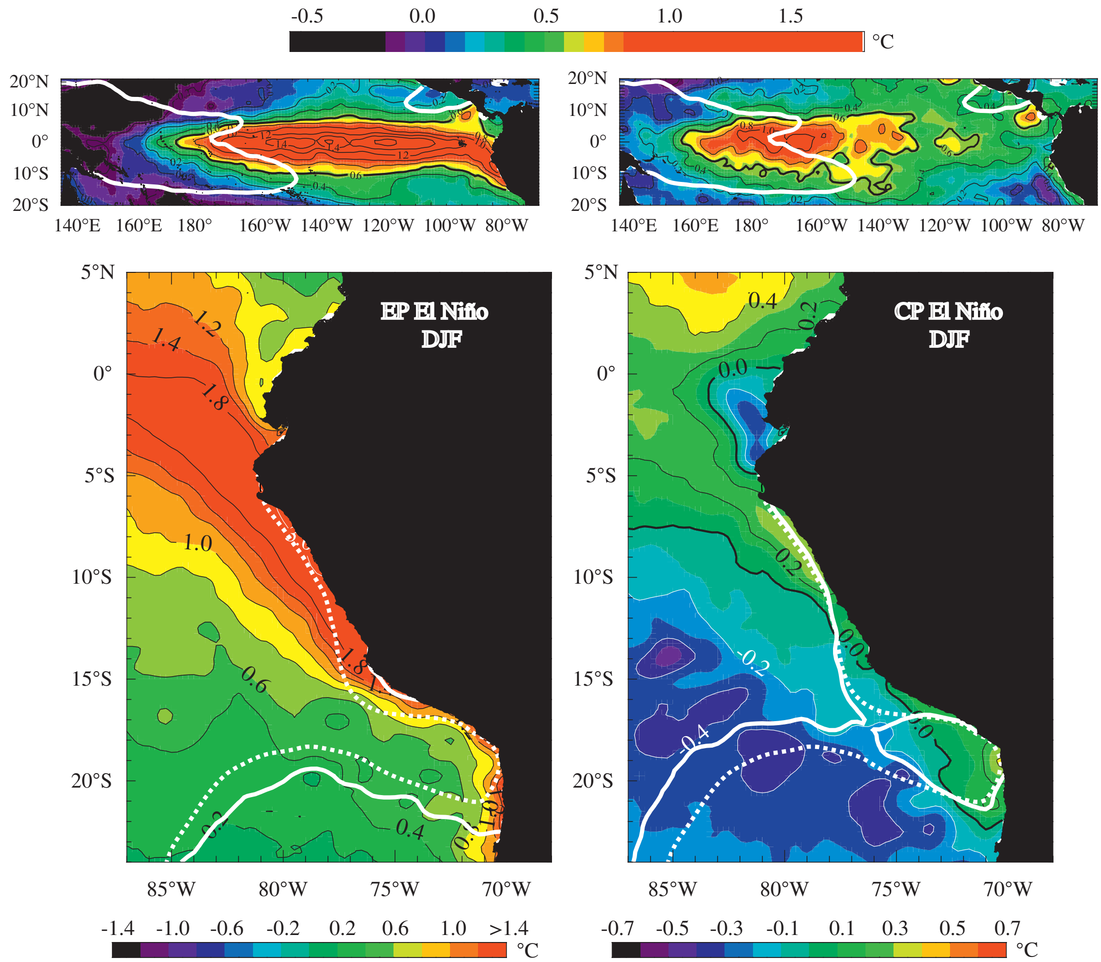

Fig. 1. DJF EP (left) and CP (right) composites of SST anomalies (top) in the tropical Pacific from HadISST data for 1900–2010 (22EP El Niños and 9 CP El Niños were used (see text)) and (bottom) along the coast of Peru from the Reynolds data for 1982–2010 (4 EP El Niño events and 9 CP El Niño events were used). Units are in °C. The white thick lines in the top panels indicate the mean position of the 28 °C isotherm (warm pool region). The white thick dotted (plain) lines in the bottom panel indicate the position of the 20°C isotherm for the mean condition (for the El Niño composite).

composites[1] for reconstructed SST anomalies from the HadISST data set (Rayner et al., 2003). Whereas during EP El Niño the convective region is displaced eastward due to increased temperature in the eastern Pacific, during the CP El Niño, the warm pool region is hardly moved and convection is increased above it due to warmer SST. In the eastern equatorial Pacific, SST anomaly is weak during CP El Niño reflecting a shallow thermocline. The different mean SST state during the two flavours of El Niño implies a different ENSO dynamics. Kug et al. (2009) suggest in particular that the zonal advective process is favored during the CP El Niño owing to the maintenance of the marked zonal SST contrast across the Pacific. The difference in dynamics of the two flavours of El Niño needs to be documented in order to get insights into the long-term trend of the tropical Pacific variability. This issue is also relevant for the understanding of the long-term trend of the upwelling along the west coast of the South America which behaves as an extension of the equatorial wave guide (Clarke and Van Gorder, 1994; Pizarro et al., 2001). Of particular interest in this study, with regards to the ENSO oceanic teleconnection, is the Humboldt Current System that experiences the most dramatic changes in its hydrology (Pizarro et al., 2002; Fig. 1) and ecosystem (Gutierrez et al., 2008) under extreme El Niño events (i.e. EP El Niño). On the other hand, during the peak of the CP El Niño the mean SST is hardly modified off the coast of Peru (slightly cooler than normal off shore, cf. Fig. 1), reflecting a shallow thermocline (or increased upwelling) and suggesting a different impact of the interannual equatorial Kelvin wave (hereafter EKW) on the upwelling.

The objective of this study is to document the characteristics of the EKW during the two flavours of El Niño in order to provide materials for the understanding of the long-term upwelling variability along the coast of Peru. The background motivation is to understand the trend in mean upwelling conditions in the Humboldt system considering that the EKW may experience a change in characteristics associated to the increased occurrence of the CP El Niño in recent years. We take advantage of long-term satellite observational records as well as an oceanic reanalysis and a high-resolution model simulation of the Peru regional circulation.

The paper is organised as follows: Section 2 presents the data sets, the methods and the high-resolution model experiment. Section 3 provides a detailed description of the EKW characteristics over the 1958–2008 period, whereas Section 4 documents the upwelling low-frequency variability and trend in the regional model experiment after providing some validation of the model interannual to decadal variability. The last section includes the discussion followed by concluding remarks.

[1] Composites were constructed following Yeh et al. (2009), i.e. based on the comparison of the values of the NINO3 and NINO4 indices during December–January–February (DJF).

Please cite this article as: Dewitte, B., et al., Change in El Niño flavours over 1958–2008: Implications for the long-term trend of the upwelling off Peru. Deep-Sea Res. II (2012), http://dx.doi.org/10.1016/j.dsr2.2012.04.011

2. Data and method

2.1. Satellite SST data

Three Sea Surface Temperature (SST) data sets are used in the study:

1) The Reynolds 25 km optimally interpolated sea surface temperature data set is produced as part of the Group for High Resolution Sea Surface Temperature (GHRSST). This product is available in daily files from September 1981 to the present. Daily files are the result of an optimal interpolation of satellite derived SST data from the Advanced Very High Resolution Radiometer (AVHRR) as well as in-situ data. All data are available through the GHRSST Global Data Assembly Center (GDAC) (Donlon et al., 2007; ftp://podaac.jpl.nasa.gov) located at NASA's Physical Oceanography Distributed Active Archive Center (PO.DAAC). More information on the interpolation may be found in (Reynolds and Smith, 1994; Reynolds et al., 2002).
2) The NOAA Version 5.0 and Version 5.1 Pathfinder AVHRR SST data set. This data set is also available from September 1981 through the end of 2010. All data are separated into nighttime and daytime daily files. For this study, to avoid issues of diurnal heating, only the nighttime files were used. The data set is not optimally interpolated and thus has data gaps predominately due to cloud cover. However the advantage is the spatial resolution of the data (4 km). The data were obtained through the NASA PO.DAAC (ftp://podaac.jpl.nasa.gov and are also available through the producer at NOAAs National Oceanographic Data Center (NODC) at ftp://data.nodc.noaa.gov). More information on the differences between version numbers and algorithm details may be obtained from Kilpatrick et al. (2001) and Vázquez-Cuervo et al. (2010). This data set was used to identify fine scale structure that might not appear in the Reynolds data and for consistency check for the high-resolution model simulation. A seasonal data set (quarterly time-series) is constructed over the period 1985–2005 through objective interpolation in order to fill in the missing values associated with cloud cover.
3) The Hadley Centre Sea Ice and Sea Surface Temperature data set (HadISST).
The Met Office Hadley Centre's sea ice and Sea Surface Temperature (SST) data, (so called HadISST1 data) are produced on monthly globally-complete fields of SST and sea ice concentration on a 1° latitude–longitude grid (i.e. ~110 km near the equator) from 1870 to date. SST data is directly taken from the Met Office Marine Data Bank (MDB). More information on this data set may be found in Rayner et al. (2003).

For the Reynolds and Hadley centre products, anomalies are relative to the mean monthly seasonal cycle calculated over 1982–2008 and 1900–2010 respectively whereas for the AVHRR SST the anomalies are relative to the mean over 1985–2005.

2.2. Wind data

In this paper, we use a wind product derived from the National Centers for Environmental Prediction–National Center for Atmospheric Research (NCEP–NCAR) Reanalysis (Kalnay et al., 1996) because of its extended period of time (1948–2008). Due to the coarse resolution of the NCEP atmospheric model ($2.5^\circ \times 2.5^\circ$) and the rough representation of the Andes, NCEP winds lead to a wind stress curl that is located too much off-shore, which prevents from using the direct model outputs for oceanic downscaling experiments. In a recent paper Goubanova et al. (2011) proposed a statistical downscaling approach to refine the resolution to $0.5^\circ \times 0.5^\circ$ and correct for the biases of the NCEP reanalyses near the Peru–Chile coasts. The statistical model is built over the period 2000–2008 based on the statistical relationship between, on the one hand, large-scale 10 m wind and sea level pressure from NCEP reanalyses and, on the other hand, regional surface wind from QuikSCAT satellite. Despite the limited span of the period over which the statistical model is trained, it provides a cost effective alternative approach to the dynamical downscaling and simulates some key aspects of the daily to interannual variability in the Humboldt region. The reader is invited to refer to Goubanova et al. (2011) for more details on the method and its validation.

2.3. SODA data

The SODA reanalysis project, which began in the mid-1990s, is an ongoing effort to reconstruct historical ocean climate variability on space and time-scales similar to those captured by the atmospheric reanalysis projects. In this paper, we used the SODA 1.4.2 version. SODA 1.4.2 uses a general circulation ocean model based on the Parallel Ocean Program numerics (Smith et al., 1992), with an average 0.25° (lat) $\times$ 0.4° (lon) horizontal resolution and with 40 vertical levels with 10 m spacing near the surface. The constraint algorithm is based on optimal interpolation data assimilation. Assimilated data includes temperature and salinity profiles from the *World Ocean Atlas-01* (MBT, XBT, CTD, and station data), as well as additional hydrography, SST, and altimeter sea level. The model was forced by daily surface winds provided by the European Center for Medium Range Weather Forecasts ERA40 reanalysis (Uppala et al., 2005) for the 44-year period from January 1958 to December 2001. Surface freshwater flux for the period 1979–present is provided by the Global Precipitation Climatology Project monthly satellite-gauge merged product (Adler et al., 2003) combined with evaporation obtained from the same bulk formula used to calculate latent heat loss. Sea level is calculated prognostically using a linearised continuity equation, valid for small ratios of sea level to fluid depth (Dukowicz and Smith, 1994). The reader is invited to refer to Carton et al. (2000) and Carton and Giese (2008) for a detailed description of the SODA system.

2.4. Tide gauge data

Tide gauge observations are used to evaluate the skill of the regional model. 6 stations, along the Peruvian coast, from Talara (4.58°S) to Matarani (17.05°S) are used. Data are provided by The University of Hawaii Sea Level Center available at (http://ilikai.soest.hawaii.edu/uhslc/data.html).

2.5. In-situ 15 °C isotherm depth data

The XBT, CTD, Niskin and Nansen bottle measurements at six fixed location from 256 IMARPE's and international cruises were gathered over the period 1961–2008 and used to derive temperature profiles in $2^\circ \times 1^\circ$ bins off the Peruvian coast between 3°S and 14°S and on a 20-m resolution vertical grid (between 0 and 200 m). This method allows deriving monthly averages with a few gaps, which are filled through linear interpolation (Flores et al., 2009). The 15 °C isotherm depth is then derived from the temperature profiles.

2.6. Estimation of equatorial Kelvin wave

The oceanic EKW was derived from the SODA reanalysis. The method for deriving the Kelvin wave is similar to Dewitte et al. (2008) and consists of projecting the simulated variability onto the theoretical vertical mode and meridional Kelvin/Rossby mode functions. The latter are derived from the SODA mean vertical stratification at each grid point along the equator and for each time step (a slowly varying density field (low pass filtered at 7 years) is considered). The reader is invited to refer to Dewitte et al. (2008) for more details about the method. The method provides an estimate of the EKW that takes into account dispersion effects associated to the zonally and temporally (low frequency) varying stratification. The monthly anomalies are referenced to the mean seasonal cycle over 1958–2008.

2.7. Regional model simulation

The ROMS (Regional Ocean Modelling System) regional ocean circulation model (Shchepetkin and McWilliams, 2005) is used at an eddy-resolving resolution (1/12° at the equator) in a study region extending from 12°N to 40°S, and from the coast to 95°W, with lateral open boundaries on its northern, western and southern sides. ROMS solves the hydrostatic primitive equations with a free-surface explicit scheme, and stretched, terrain-following sigma coordinates on 37 vertical levels. Subgrid-scale vertical mixing is parameterized using the KPP boundary layer scheme (Large et al., 1994). Bottom topography from GEBCO global 30 arc-second grid data set (http://www.gebco.net/data_and_products/gridded_bathymetry_data/documents/gebco_08.pdf) has been interpolated onto the model grid, smoothed as in Penven et al. (2005) in order to reduce pressure gradient errors and modified at the open boundaries to match with bottom topography from the boundary forcing provided by SODA (see Fig. 2).

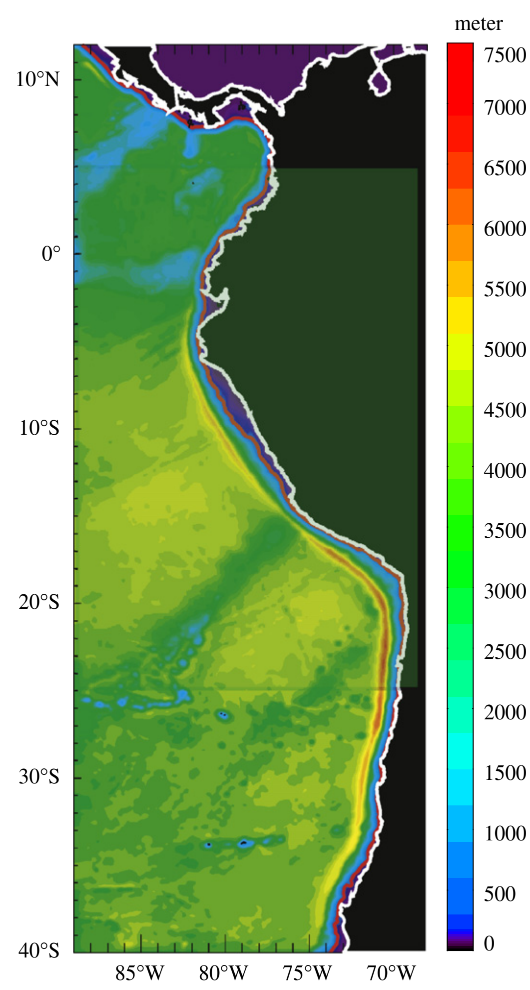

Fig. 2. Model domain and topography. The shaded zone indicates the domain over which we focus our analysis. The red contour indicates the 300 m isobath. (For interpretation of the references to color in this figure legend, the reader is referred to the web version of this article.)

5-daily mean oceanic outputs from SODA provide the open boundary conditions (OBC) for temperature, salinity, horizontal velocity and sea level over the period 1958–2008. They were treated using a combination of an Orlanski scheme for the tracers and for baroclinic velocities and a Flather scheme for the barotropic mode (Marchesiello et al., 2001). Initial conditions are from the 1st of January, 1958 and a 3-year spin-up was performed by repeating the year 1958.

To force the regional model at the air/sea interface, wind speed and wind stress from the downscaled product of Goubanova et al. (2011) were used (see above). Atmospheric fluxes were derived from the bulk formula using the air temperature from COADS 1° monthly climatology (daSilva et al., 1994). Short wave and long wave radiations as well as relative humidity are from COADS. This choice is motivated by the large biases observed in the NCEP atmospheric fluxes near the coast of the Peru and Chile.

Within this configuration, the model simulates a realistic mean SST although with a cool bias in the coastal region (see Fig. 3, left panels) that is attributed to the use of COADS climatology for short wave radiation that tends to cool the SST during El Niño conditions. The model also simulates an overall realistic pattern of mean Eddy Kinetic Energy (EKE) (Fig. 3, right panels) which indirectly reflects a realistic vertical current structure (Fig. 3f) that is characterised by a well defined Peru Undercurrent Current (PUC) (see Huyer et al. (1991) and Montes et al. (2010) for a comparison). The comparison of the model mean EKE and the mean EKE estimated from altimetry is somehow limited due to the different resolution of the products. Further validation of the model from observations is provided in Table 1 (from tide gauge data) and in Section 4.

The simulation is used here to extend the composite analysis from the SST observations to some aspects of the regional circulation, which includes the upwelling (vertical velocity), thermocline depth along the coast and along-shore current vertical structure (see Section 4).

2.8. Definition of El Niño types

To separate the EKW characteristics during the two flavours of El Niño, a composite analysis is used. The CP and EP years are selected using the method proposed by Yeh et al. (2009), namely based on the values of the NINO3 and NINO4 indices with a threshold of 0.5 °C during the NDJ season to define that an El Niño is occurring. Over 1958–2008, this leads to the selection of 6 CP events (1968–69, 1990–91, 1994–95, 2002–03, 2004–05, 2006–07) and 5 EP events (1965–66, 1972–73, 1976–77, 1982–83, 1997–98). Unless stated otherwise, the 1986–87 event is not considered in the analysis because this event evolves as an EP event at the developing phase and turns toward the CP type at the mature phase.

The significance of composites was estimated using the bootstrap method (Efron, 1982). The method is equivalent to a Monte-Carlo testing (cf. Björnsson and Venegas, 1997) and consists of creating a surrogate data, a randomized data set of CP (6) and EP (5) events by scrambling 51 years in the time domain. The composite analysis is then performed on the scrambled data set. The same procedure of scrambling the data set and performing the analysis is repeated 300 times, each time keeping the value of the CP and EP composites (in the space and time domains). Then the difference between CP and EP composites is calculated for the 300 samples and the distribution of these

Please cite this article as: Dewitte, B., et al., Change in El Niño flavours over 1958–2008: Implications for the long-term trend of the upwelling off Peru. Deep-Sea Res. II (2012), http://dx.doi.org/10.1016/j.dsr2.2012.04.011

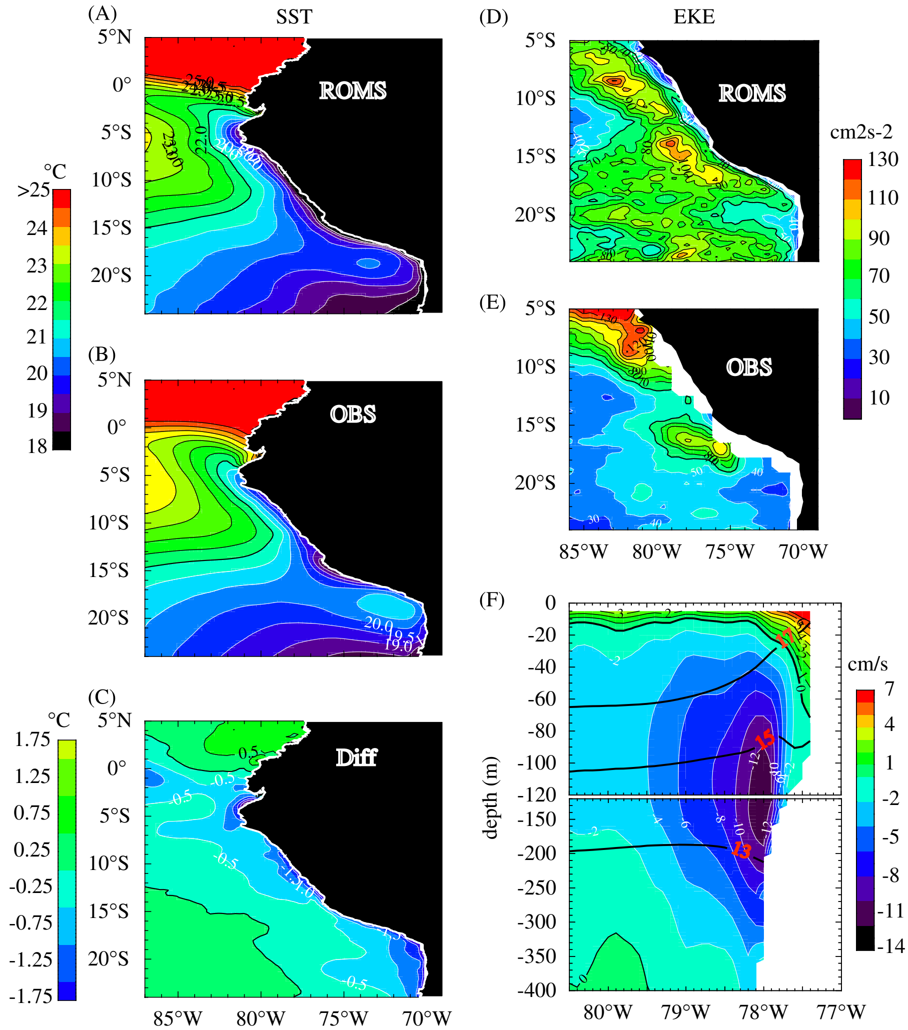

Fig. 3. Mean SST (A, B) and mean EKE (D, E) for model (A, D) and observations (B, E). C) The difference between model and observations for SST. The periods are 1982–2008 for SST and 1993–2008 for EKE. Units are °C for SST and $cm^2\,s^{-2}$ for EKE. EKE is derived from geostrophic surface velocity interannual anomalies. Observations are the Reynolds data for SST and the merged altimetric products from TOPEX/Poseidon, JASON 1 and ERS1/2 provided by CLS (Collecte Localisation Satellites). (F) Mean alongshore simulated current at 12°S as a function of depth and longitude over 1958–2008. The 13 °C, 15 °C and 17 °C mean isotherm are displayed in thick black line. Contour interval is every 2 cm/s (1 cm/s) for poleward (equatorward) currents.

Table 1
Comparisons between monthly model sea level interannual anomalies (SLA) and gauges data at different stations along the coasts of Peru. SigmaF is the ratio RMS(MOD)/RMS(OBS) where RMS is the Root Mean Square, and the score is estimated following Eq. 4 from Taylor (2001). SLA are estimated with respect to the nine-year monthly climatology from January 1995 to December 2003.

	R	SigmaF	Score	Rms diff	Rms (OBS)	Rms (MOD)	Period
Talara (4.58°S)	0.4536	0.6282	0.5898	8.225	9.057	5.689	Dec. 1987–Sept. 2008
Païta (5.08°S)	0.4660	0.7204	0.6595	7.592	8.247	5.941	Dec. 1987–July 2008
Callao (12.02°S)	0.7047	0.7625	0.7927	4.949	6.952	5.301	Jan. 1970–Sept. 2008
Pisco (13.71°S)	0.6434	0.5863	0.6257	6.553	8.536	5.005	Jan. 1991–Dec. 2007
San Juan (15.36°S)	0.5880	0.5323	0.5464	5.889	7.264	3.867	Jan. 1978–Dec. 2002
Matarani (17.05°S)	0.4405	0.5649	0.5283	6.570	7.249	4.095	Jan. 1992–Sept. 2008

differences is obtained. The latter is used for deriving the significance level of the composites.

3. Equatorial Kelvin wave during the two flavours of El Niño

Fig. 4 presents the composite analysis of the first baroclinic mode EKW for the two types of El Niño. The year 0 refers to the year preceding the peak phase. The comparison reveals a contrasted behaviour: The EP composite exhibits clear eastward propagation features reflecting the recharge-discharge process (Jin, 1997) whereas the CP composite resembles a standing basin mode with a weak cool phase. The other well identified difference is the amplitude of the downwelling (positive) EKW which is much weaker for the CP composite particularly in the far eastern Pacific. Because of the sloping thermocline from west to east in the equatorial Pacific, the oceanic variability also projects significantly onto the second baroclinic mode (Dewitte et al., 1999). Fig. 5 displays the seasonal evolution of the EKW of the second baroclinic mode for the two types of El Niño. It also indicates a

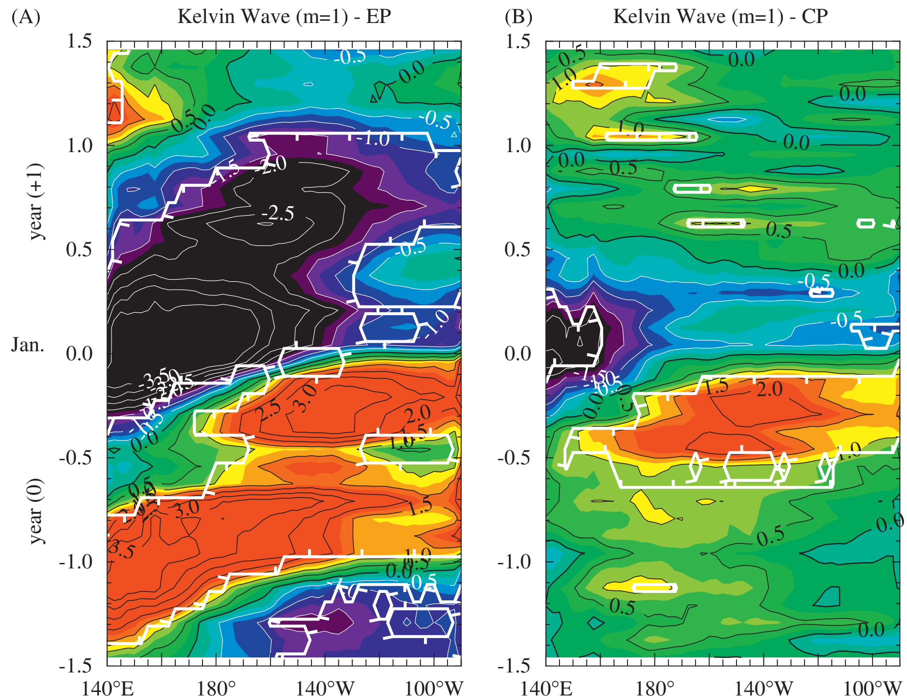

Fig. 4. Composite evolution of the first baroclinic mode Kelvin wave during EP (A) and CP (b) years along the equator. Unit is cm. The contour in thick white line indicates the 90% significance level.

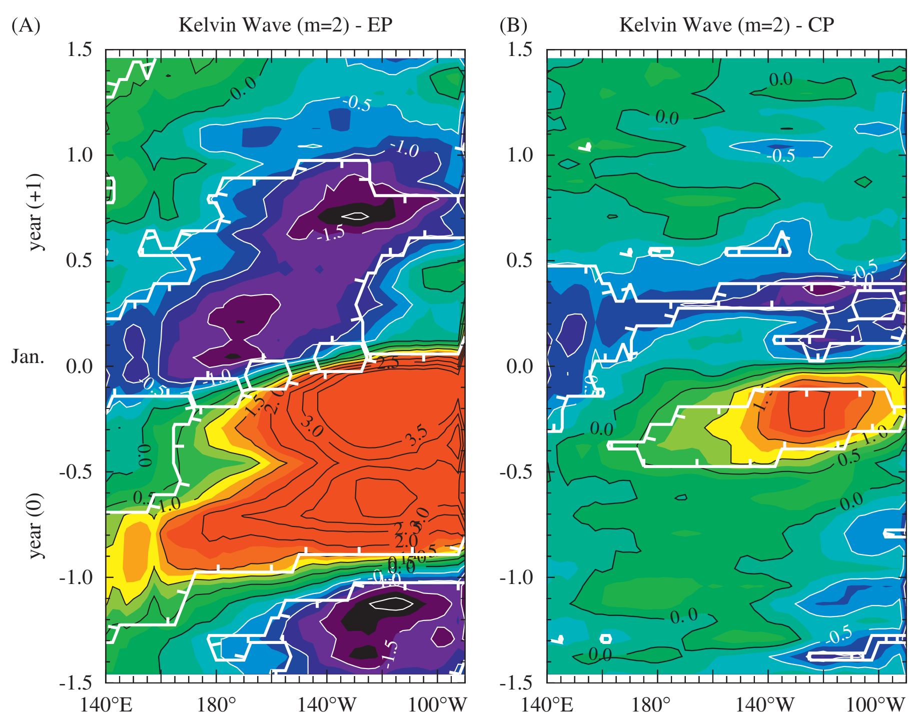

Fig. 5. Same as Fig. 4 but for the second baroclinic mode Kelvin wave.

different anomaly pattern for CP and EP El Niños although both composites have a peak anomaly in the eastern Pacific reflecting the vertical mode dispersion associated with the shallowing thermocline as the waves propagate to the east. Like for the first baroclinic mode, the amplitude of the downwelling EKW during the EP event is larger than for the CP event. However the ratio of the maximum amplitude between El Niño types is much larger for the second baroclinic mode, reaching 7 instead of 2 for the first baroclinic mode. Also, the downwelling EKW is followed by an upwelling EKW for the CP event, which is different from the first baroclinic mode and from the EP composite of the second baroclinic mode EKW. Such differences between El Niño types

Please cite this article as: Dewitte, B., et al., Change in El Niño flavours over 1958–2008: Implications for the long-term trend of the upwelling off Peru. Deep-Sea Res. II (2012), http://dx.doi.org/10.1016/j.dsr2.2012.04.011

are further illustrated in Fig. 6 which displays the evolution of the second baroclinic mode EKW at 90°W. EKW amplitude has been normalised by the maximum amplitude of the EKW at the peak phase of the event in order to emphasise the difference in time spans of downwelling and upwelling. It is clear that the EKW for CP event has a tendency towards upwelling rather than downwelling conversely to the EP event. The skewness of the (normalised) EKW over the ENSO cycle is 4.07 cm (0.68) and −0.62 cm (−0.45) for EP and CP events, respectively.

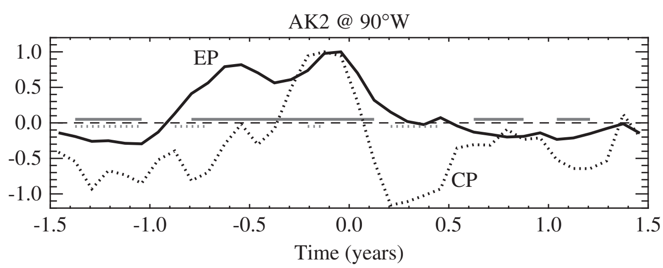

Fig. 6. Composite evolution of the second baroclinic mode Kelvin wave during EP (a) and CP (b) years at 90°W. The amplitude of the Kelvin wave is adimentionalized by the maximum value. The full (dotted) grey horizontal line indicates where the EP (CP) composite is significant at the 90% level.

Summarizing, our results indicate that the EKW exhibits different characteristics during CP and EP El Niño, with a different asymmetry and distinct vertical structure variability in each case. In particular, the EKW of the first baroclinic mode may weakly impact the Peru upwelling system during CP event due to its basin mode pattern, which is in contrast with the first baroclinic mode EKW during EP event that has a strong positive asymmetry in the eastern Pacific. The second baroclinic mode EKW during CP events is negatively skewed near the Ecuadorian coast whereas its EP El Niño counterpart is strongly positively skewed.

4. Impact on the regional circulation off Peru

4.1. EP and CP conditions

In this section, we take advantage of a long-term regional model experiment to extend the previous analysis to some aspects of the regional circulation off Peru. Of particular interest are the upwelling variability characteristics during the two flavours of El Niño. As a first step, we present some validation of the model interannual to decadal variability. Then the model outputs are used to document the EKW impact on the coastal upwelling and its long-term trend.

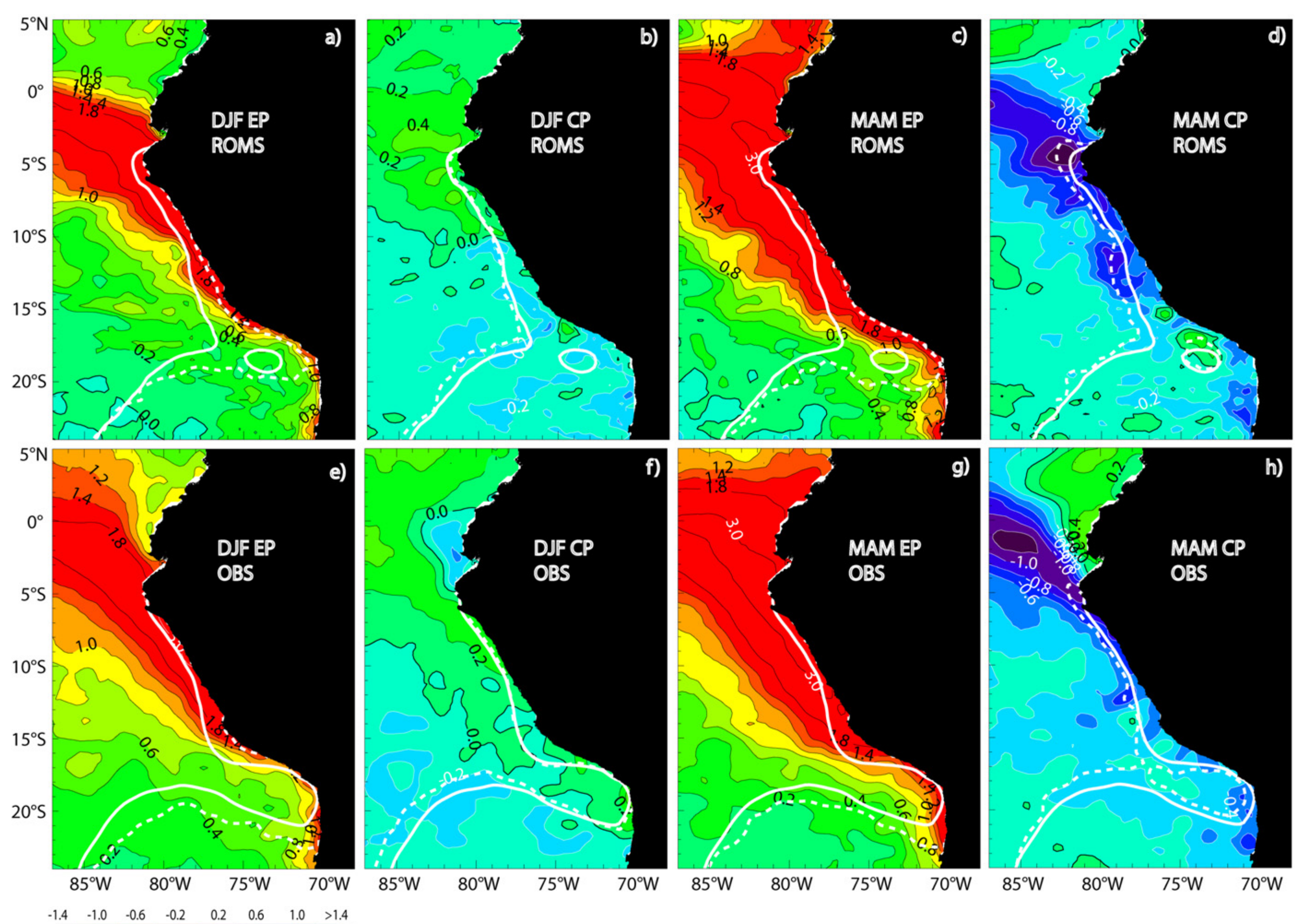

Fig. 7. CP and EP composites for SST for (top) the model and (bottom) the observations (Reynolds data) during the DJF and MAM seasons. Due to the limited number of events over 1982–2008, the 1986–87 El Niño is considered here in the EP composites. The thick plain white line indicates the mean position of the 20 °C isotherm whereas the dashed white line refers to the position of the 20 °C isotherm during anomalous conditions. Units are in °C and contour intervals are every 0.2 °C below 1.4 °C (see colour bar in the bottom hand corner). (For interpretation of the references to color in this figure legend, the reader is referred to the web version of this article.)

Fig. 7 presents the CP and EP composites of SST for the observations and the model for the December–January–February and the March–April–May seasons. It indicates that the model simulates realistically the evolution of the CP and EP El Niño events near the peak phase. The spatial correlation between model and observed composites is above 0.6 for both seasons and El Niño types. The main deficiencies of the model are the weaker amplitude of warm anomalies during EP El Niño and the slightly warmer SST during CP El Niño in the equatorial region for the seasons corresponding to the peak phase in December–January–February (DJF) and the decaying phase in March–April–May (MAM). The slightly weaker amplitude of the model variability in comparison with the observations is also observed for the sea level (see Table 1). These biases are likely due to the use of COADS climatology for calculating heat fluxes and the biases in downscaled wind fields (Goubanova et al., 2011) that in one case tends to cool the SST through anomalous short wave flux during El Niño and in the other case does not account properly for the wind-evaporation-SST feedback mechanism in the near equatorial region. Sensitivity tests using atmospheric fluxes from a dynamical downscaling experiment with the WRF model (Skamarock et al., 2005) indicate that the discrepancies between observations and model for SST is largely due to the heat flux forcing (not shown), consistent with the above interpretation. Since we are interested in upwelling variability (and not just SST variability) and given that the simulation using the statistically downscaled winds extends over a long period of time, it is appropriate for the following analyses. As a final validation for SST, and since we will investigate low frequency variability and trend in the following section, we diagnose the decadal mode for SST based on Empirical Orthogonal Function (EOF) analysis. Fig. 8 presents the dominant mode of the 7-year low pass filtered SST and associated time-series for the model, the Reynolds data and the Pathfinder data. Despite the discrepancies between the observed data sets which results from the different resolution that has been noticed in previous studies for other regions (Reynolds and Chelton, 2010; Vázquez-Cuervo et al., 2010), the results of Fig. 8 suggest that the model is able to capture the magnitude, phase and pattern of the SST decadal variability. Differences in the first EOF between the Reynolds and Pathfinder 4 km product are likely due to decadal variability that is associated with higher spatial scales, such as movement of the upwelling fronts and mesoscale to sub-mesoscale variability. The pathfinder 4 km data more closely reflects the pattern of the decadal signal seen in the ROMS model, which indicates that higher spatial resolution is needed to fully capture the coastal dynamics, even at the decadal scale.

We now focus on subsurface variability. Fig. 9 presents a comparison between model and observations for subsurface temperature. The 15 °C isotherm depth is used here as a proxy for thermocline depth near the coast. It indicates that the model simulates reasonably the along-shore thermocline depth, which includes the meridional gradient. For instance, during the peak phase of the EP El Niño the thermocline is as deep as 180 m at 4°S and shallows to 120 m at 14°S for both model and observations. Although there is a tendency for the model to simulate a too shallow thermocline compared to the observations, the model–data misfit is not as large as for the SST reflecting that subsurface temperature is less sensitive to biases in heat fluxes forcing. Note that during the CP El Niño, the mean thermocline depth is close to its climatological position, which favours the propagation of high-order baroclinic mode waves compared to the EP El Niño condition.

In order to evaluate to what extent the EKW can impact the thermocline variability along the coast, similar composite analyses than above (Section 3) are performed. Fig. 10 presents the evolution of the thermocline variability along the coast during EP and CP El Niño years. The deviation from the mean climatological state (presented in Fig. 10C) is considered here. Fig. 10 reveals a contrasted situation during the CP and EP El Niño, with the thermocline deepening sharply during EP event from March (Year −1) to May (Year 0) while slightly deepening by a few tens of metres north of 15°S during the CP event at the peak phase of the event. Like for the EKW, the two flavours or types of El Niño are characterised here by pronounced different asymmetries over the ENSO cycle, with the thermocline anomalies having a negative

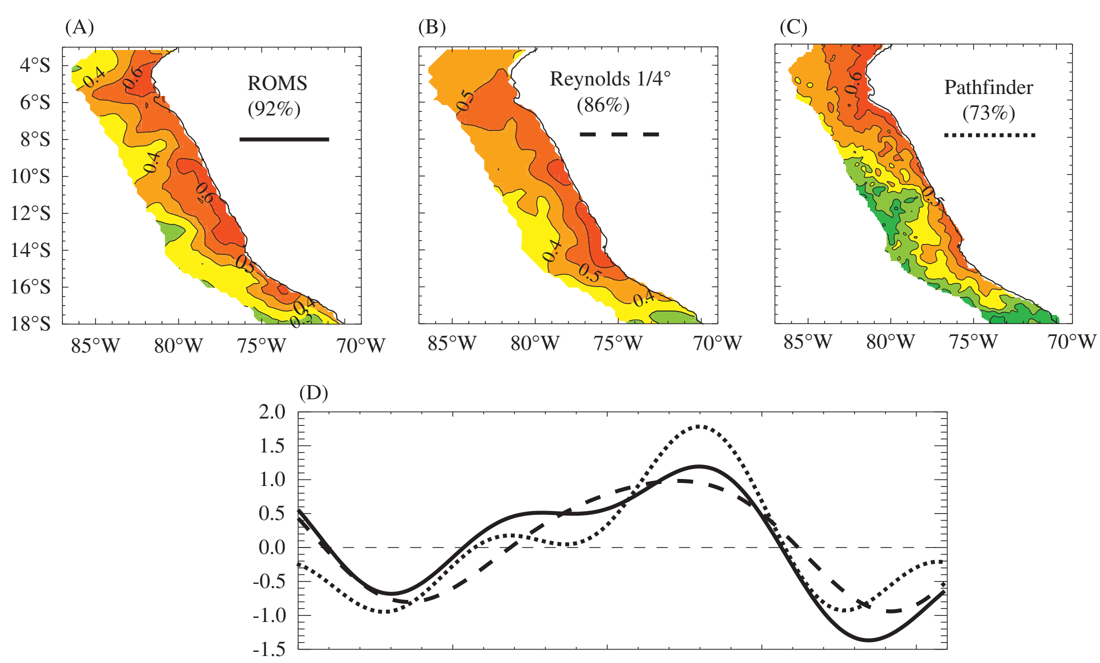

Fig. 8. First EOF mode of 7-year low pass filtered SST anomalies: (A) ROMS, (B) Reynolds data and (C) Pathfinder 4 km data along the coast between 3°S and 18°S. The ROMS outputs were previously interpolated on the 1/4° × 1/4° Reynolds data grid whereas the mode pattern derived from GHRSST-PP data was averaged twice over a 4 by 4 box in order to smooth out details. (D) Associated time series for ROMS (plain full line), Reynolds data (dashed line) and the GHRSST data (dotted line).

Please cite this article as: Dewitte, B., et al., Change in El Niño flavours over 1958–2008: Implications for the long-term trend of the upwelling off Peru. Deep-Sea Res. II (2012), http://dx.doi.org/10.1016/j.dsr2.2012.04.011

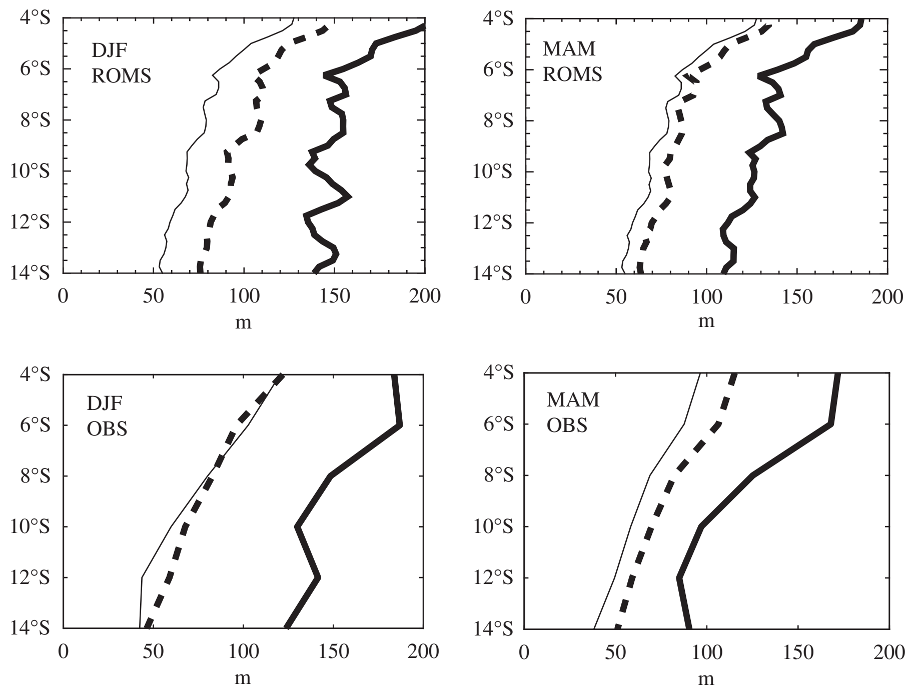

Fig. 9. CP (thick dotted line) and EP (thick plain line) composites for mean thermocline depth (15 °C isotherm depth) along the coast of Peru between 4°S and 14°S (bottom) as derived from the historical regional cruise of IMARPE and (top) for the model. The thin plain line represents the mean position of the thermocline over the period 1958–2007.

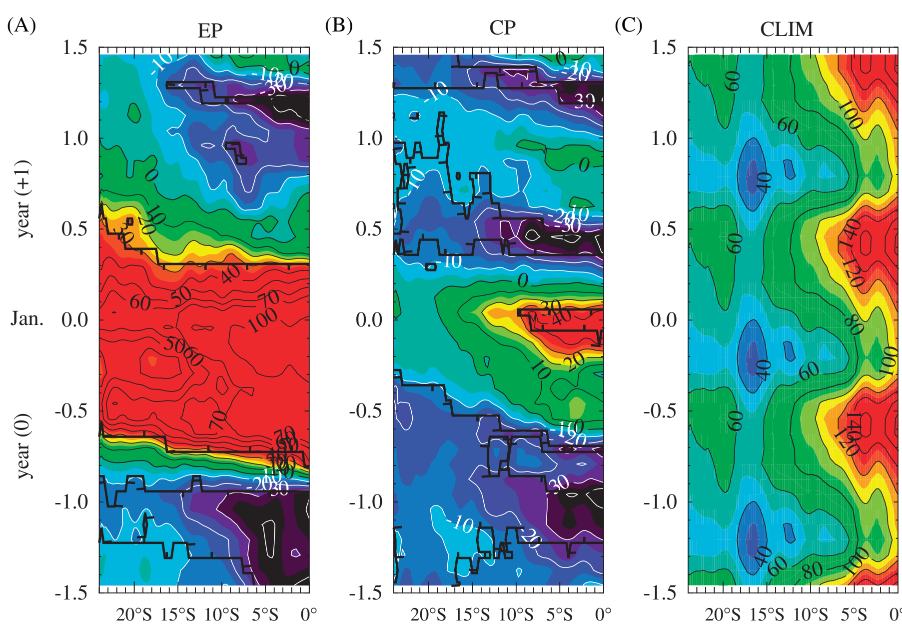

Fig. 10. Composite evolution of the 15 °C isotherm depth anomalies wave during the EP (A) and CP (B) years along the coast of Peru. The contour in thick black line indicates the 90% significance level. (C) Climatological fluctuations of the 15 °C isotherm depth. Unit is metre.

skewness during CP El Niño and a strong positive skewness during EP El Niño.

4.2. Decadal variability and long-term trend

The different mean state during the two flavours of El Niño has implications for the interpretation of the long-term trend of SST in this region. Observational records suggest a cooling trend off the coast of central Peru (Gutierrez et al., 2011a, 2011b) although trends in upwelling favourable winds remain ambiguous due to the quality of the data sets (Goubanova et al., 2011; Gutierrez et al., 2011a, 2011b). The increase of occurrence of CP El Niño in recent decades (Lee and McPhaden, 2010) suggests that mean to cool conditions have been favoured off the coast of Peru due to reduced amplitude of the downwelling EKW and negative skewness of the EKW over an ENSO cycle (Fig. 5). This implies that EKW may be influential on the mean condition through its residual effect on the mean SST. In order to test this hypothesis,

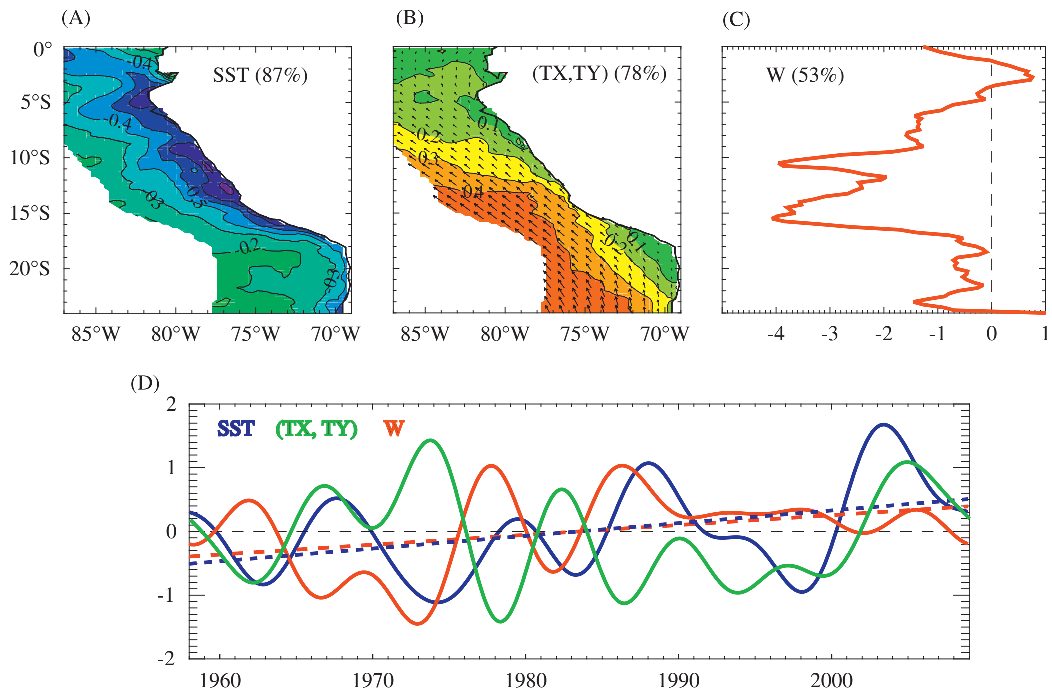

Fig. 11. EOF analysis of low-frequency SST, wind stress and upwelling in the model: first EOF mode for (A) SST, (B) zonal and meridional wind stress and (C) coastal upwelling. See text for the method for estimating coastal upwelling. (D) Time series associated to the first EOF mode for (blue) SST, (red) coastal upwelling rate and (green) wind stress. The linear trend for SST (upwelling) EOF time series is plotted in thick blue (red) dashed line in (D). The amplitude of the anomalies in dimensional unit corresponding to the low frequency mode can be inferred by multiplying the value of the time series with value of the corresponding EOF mode pattern. In that case, units are °C for SST, 0.01 N m^{-2} for wind stress and 10^{-6} m/s for upwelling rate. (For interpretation of the references to color in this figure legend, the reader is referred to the web version of this article.)

Table 2
Correlation between EOF time series associated to the low frequency modes for SST, wind stress (TX, TY) and upwelling rate (W) (cf. Fig. 11) for different periods of time.

	1958–2008	1958–1986	1987–2008
⟨W|SST⟩	0.24	0.17	−0.07
⟨W|TXTY⟩	−0.75	−0.93	−0.40
⟨SST|TXTY⟩	+0.11	−0.33	0.67

we use the model outputs and diagnose as a first step the decadal variability of SST, wind stress and upwelling rate. The latter is estimated from the maximum vertical velocity in the depth range of 0–80 m at the first grid point near the coast (which corresponds to a ~8-km wide coastal band) following Marchesiello and Estrade (2010). Fig. 11 presents the results of the EOF analysis of the 7-year low-pass filtered fields. It indicates that there is a cooling trend in the model that does not result in a straight forward manner from wind-induced upwelling since the wind stress decadal mode does not exhibit any trend at all (not plotted in Fig. 11D). The trend for the decadal mode of SST is 0.19 unit per decade (10 yr^{-1}) which is significant (with a standard error for the slope of $\pm 0.013 \times 10$ yr^{-1} assuming Gaussian measurement errors at each point of the time series). Also, the EOF time series of low-frequency SST and upwelling rate are uncorrelated over the whole period (Fig. 11D, cf. Table 2). The inspection of Fig. 11D reveals that there is a shift in the relationship between the low frequency upwelling rate and wind stress modes around 1986 with upwelling being highly anti-correlated to wind stress before 1986 and not after (Table 2). It was checked that upwelling rate is mostly accounted for by Ekman transport and pumping associated with the wind variability before 1986. On the other hand, after 1986 the low frequency mode for SST becomes correlated to the low frequency mode for wind stress indicating that Ekman pumping and transport cannot explain alone the SST low-frequency variability over this period. During the last two decades, the decadal mode for SST also exhibits an amplitude modulation that may reflect the change in EKW characteristics. On the other hand, the coastal upwelling is weakly modulated over the last two decades suggesting a compensation of Ekman-induced upwelling by the equatorial variability in the form of EKW activity modulation. Noteworthy, the EOF1 pattern for SST has a minimum amplitude (cooling tendency) within a narrow coastal fringe (especially marked south of 15°S), reminiscent of the influence of coastal trapped-Kelvin wave.

The change in the relationship between SST and wind stress from before and after 1986 and the absence of long-term trend in the wind stress forcing indicate that the cooling trend of the coast of Peru in the model has to result from change in equatorial oceanic variability and/or non-linear processes. We hypothesise here that the increased occurrence of the CP El Niño over the last decades (Takahashi et al., 2011) results in a long term trend of the equatorial forcing asymmetry that has a residual effect on the mean SST along the coast of Peru. This is likely if the mean SST change is related to the mean SST asymmetry off the coast of Peru. Fig. 12 presents the dominant singular value decomposition (SVD) mode between the 10-year running mean SST and the 10-year running skewness SST which explains 73% of the covariance. The comparable mode patterns and the highly correlated SVD time series (c=0.89) indicate that both quantities are related, which supports the above interpretation of the residual effect of the changing EKW forcing on the mean condition off Peru. As a consistency check we also verified that the time series obtained by projecting the decadal SST mode (Fig. 11A) onto the SST interannual anomalies has a positive trend of its 15-year running mean (i.e. cooling tendency) and skewness (i.e. reduction of positive asymmetry).

ARTICLE IN PRESS

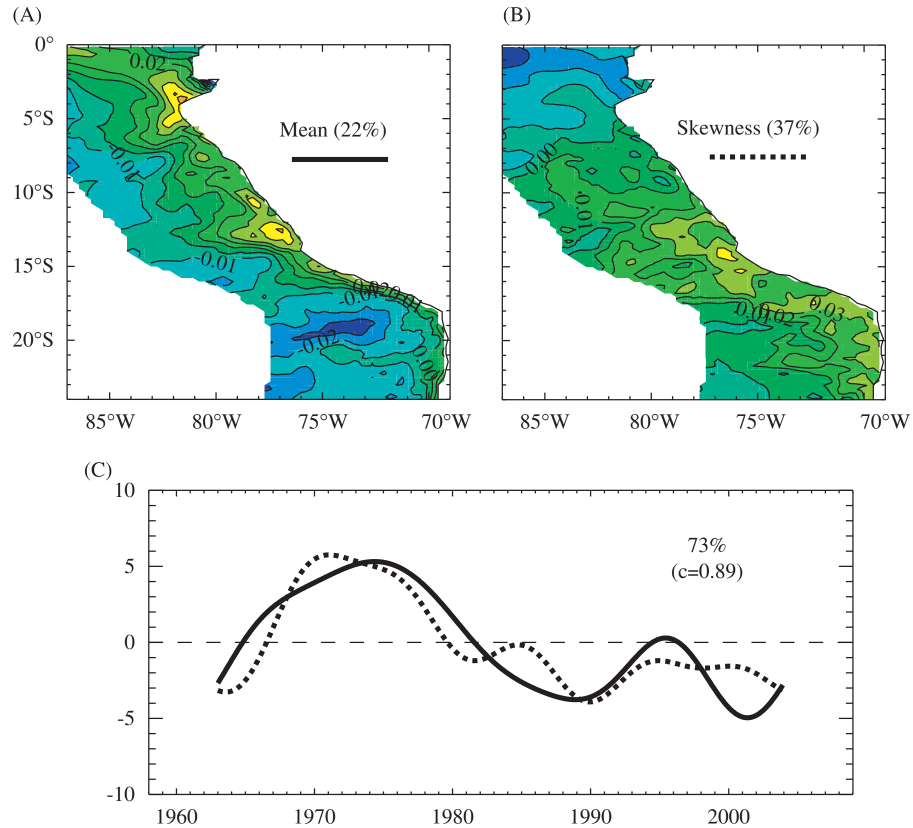

Fig. 12. Dominant SVD mode between the 10-year running mean SST and the 10-year running skewness SST: spatial patterns for the mean (A) and the skewness (B). The percentage of the total variance explained by the mode is indicated. (C) Associated time series for the mean (plain line) and the skewness (dotted line). The running mean and skewness time series were low-pass filtered with a frequency cut-off of 7 yr^{-1} before performing the SVD analysis. Multiplying the spatial pattern with the associated time series leads to a field having °C as a unit. The percentage of the total covariance between the mean and skewness explained by the mode and the correlation between the time series are indicated.

5. Discussion and conclusion

The SODA oceanic reanalysis and a high-resolution model experiment were used to study the characteristics of EKW and its connection with the coast of Peru. The focus was on the change in characteristics under the mean conditions associated with the two types of El Niño, considering that the EKW characteristics (amplitude, asymmetry and vertical structure) may be distinctively altered during both types of events. It is shown that, for EP El Niño, the EKW is characterised by a large positive asymmetry for both baroclinic modes whereas during CP El Niño, the second baroclinic mode EKW is negatively skewed over the ENSO cycle in the eastern Pacific and the first baroclinic mode EKW has a basin scale structure with a weak amplitude near the eastern boundary. These characteristics are consistent with the results of Dewitte et al. (2011a) who analysed the EKW characteristics in a long term coupled simulation that accounts for many features of the EP and CP dynamics (Kug et al., 2010). In particular, during EP El Niño, the first two baroclinic modes have comparable contribution to the recharge–discharge process (Jin, 1997) whereas during CP, the recharge–discharge process is less effective due to the basin mode pattern of the first baroclinic mode.

A high-resolution regional oceanic model simulation is then performed. It uses the SODA data as open boundary conditions. The simulation is shown to reproduce realistically many aspects of the mean circulation and interannual variability. In particular, despite the use of climatological heat flux forcing, the model simulates CP and EP SST composites that are consistent with satellite data. The composite analysis reveals in particular that, at the peak phase (DJF) of the CP El Niño, the mean SST is close to its seasonal value while during the decaying phase (MAM), the SST is cooler than normal all along the coast of Peru. This to some extent is reflected in the subsurface conditions as evidenced by the mean thermocline depth (15 °C isotherm depth) estimated from the model and the in-situ observations (Fig. 9). Thus, the mean condition during CP El Niño may favour the rectification of the mean SST by the interannual EKW since the thermocline remains relatively shallow during the whole El Niño cycle. Such process is likely if the coastal SST variability is skewed (asymmetrical) in relation to the skewed equatorial forcing. We verified that mean SST changes off Peru co-vary with the SST asymmetry low-frequency modulation, which suggests the cumulative process of cool (less warm) SST anomalies on the mean SST in relation to the increase occurrence of CP El Niño in the recent decades. As a consistency check, and to verify that this argument can be transposed to the coastal dynamics, we compare the vertical along-shore current pattern at 12°S during EP and CP events with the dominant EOF mode of the low-frequency along-shore currents (Fig. 13). The results indicate that the change in vertical structure of the along-shore current has a comparable pattern for the CP event and the decadal mode (spatial correlation between the decadal mode and the composites is 0.88 and 0.41 for CP and EP events respectively), which suggests that the increased occurrence of the CP El Niño has a residual effect on the mean current conditions off Peru. The change in vertical structure of the along-shore current during CP El Niño is favourable to the reduction in baroclinic instability since both the surface current and the base of the PUC are reduced (Fig. 13C), reducing the current shear near the coast (Marchesiello et al., 2003). Vertical stratification is also reduced during CP events along the coast (Fig. 13C). A reduction

Please cite this article as: Dewitte, B., et al., Change in El Niño flavours over 1958–2008: Implications for the long-term trend of the upwelling off Peru. Deep-Sea Res. II (2012), http://dx.doi.org/10.1016/j.dsr2.2012.04.011

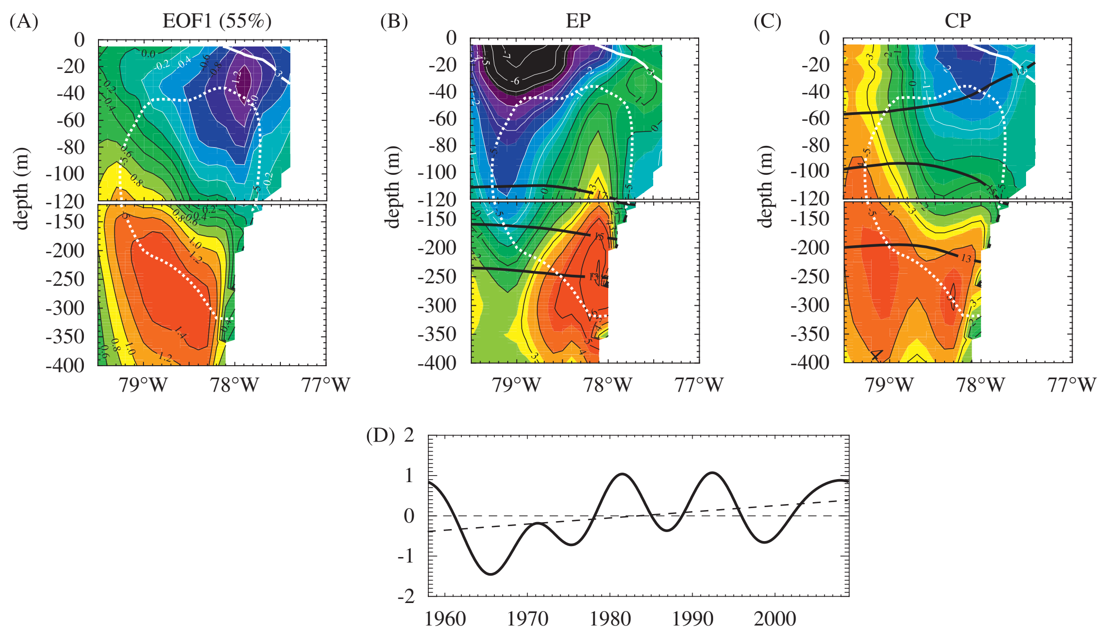

Fig. 13. (A, D) Dominant EOF mode of the 10-year low-pass filtered along-shore current anomalies at 12°S. Spatial pattern (A) and associated time series (D). Multiplying the spatial pattern with the associated time series leads to a field having cm/s as a unit. The mean along-shore current is displayed for the coutours equal to 5 cm/s (poleward—dotted thick white line) and −3 cm/s (equatorward—plain thick white line). (B, C) Composites of along-shore current anomalies for EP (B) and CP (C) events at 12°S. Units is in cm/s. The mean along-shore current is displayed for the coutours equal to 5 cm/s (poleward—dotted thick white line) and −3 cm/s (equatorward—plain thick white line). The composite of the 13 °C, 15 °C and 17 °C are also displayed in thick black lines.

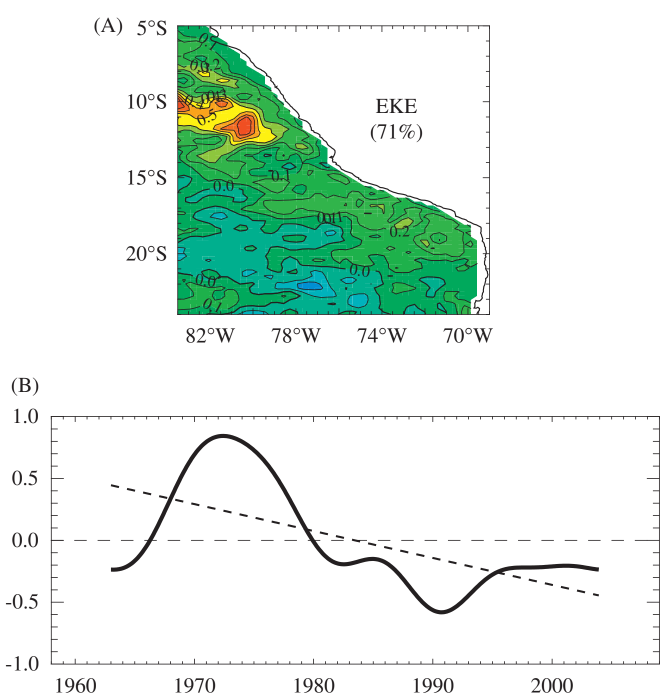

Fig. 14. Dominant EOF mode of the 10-year running mean of EKE: spatial pattern (A) and associated time series (B). Multiplying the spatial pattern with the associated time series gives a field having 100 $cm^2 s^{-2}$ as unit.

of EKE is expected in such an anomalous coastal mean state, which is observed in the model (Fig. 14).

Our results have implications for the interpretation of the long-term trend of SST in this region. Observational records suggest a cooling trend off the coast of central Peru (Gutierrez et al., 2011a, 2011b) although trends in upwelling favourable winds remain ambiguous due to the quality of the long-term data sets (Goubanova et al., 2011; Gutierrez et al., 2011a, 2011b). The increase of occurrence of CP El Niño in recent decades (Yeh et al., 2009; Lee and McPhaden, 2010) suggests that mean to cool conditions have been favoured off the coast of Peru due to the change in EKW characteristics. The absence of increasing trend of the along-shore wind stress in our experiment does not however exclude its role on the long-term trend of upwelling considering that the low-frequency modulation of wind stress could also contribute to a rectified effect on the mean SST through non-linearities. Although this is unlikely, it deserves further investigation which is beyond the scope of the present paper.

We now discuss limitations of the study as well as perspectives to this work. We have not considered in this study the role of the intraseasonal equatorial Kelvin wave (IEKW), which is influential on the upwelling variability off Peru (Dewitte et al., 2011b) and might also participate in the rectification process proposed in this study (see Belmadani et al. (2012) for the 1992–2000 period). In particular, due to the strong seasonal dependence of the intraseasonal atmospheric variability with ENSO (Hendon et al., 2007) and its amplitude modulation by the ENSO phase (Roundy and Kravitz, 2009), the IEKW activity is likely altered during the two flavours of El Niño. The analysis of a previous version of the SODA reanalysis also suggests a positive trend of the IEKW activity from the 1950s (Dewitte et al., 2008; Gutierrez et al., 2011b) although there is still a debate whether atmospheric reanalyses can reproduce the low-frequency modulation of the intraseasonal variability considering the non-homogeneous datasets that are assimilated (see Jones and Carvalho (2006)). Further study is required to document this issue.

Another limitation arises from the use of the statistically downscaled product combined with the COADS climatological data to force the oceanic regional model. In particular, Goubanova et al. (2011) show that although the downscaling method captures some aspects of the El Niño–La Niña asymmetry, it tends to underestimate the amplitude of the upwelling favourable winds during EP El Niño. Also the statistical method to derive wind speed from NCEP Reanalysis does not take explicitly into account the regional air–sea interactions which may be at work at

ARTICLE IN PRESS

intraseasonal to interannual timescales. For instance, Dewitte et al. (2011b) show that in the Northern Peru region, there is a component of the intraseasonal winds that, rather than forcing, actually responds to SST changes (see also Chelton et al. (2004) for this issue). There is also modelling evidence that the winds respond to local SST anomalies during EP El Niño off the coast of Peru (K. Takahashi, personal communication). The consideration of such processes implies the use of more realistic atmospheric forcing or of a regional coupled model. This is planned for future work.

Overall our results bring new material for the understanding of the long-term trend in the Peru upwelling. Whereas previous studies have focused on the processes of upwelling variability by the winds to explain long term trends (Bakun, 1990; Bakun and Weeks, 2008), we suggest here that the oceanic component of the tropical variability may come into play considering that the EKW activity has significantly different characteristics during the two flavours of El Niño and that the change in El Niño asymmetry implies a rectified effect on the mean upwelling condition off Peru. Future work will be dedicated to the investigation of such process based on high-resolution coupled general circulation model.

Acknowledgments

Most parts of this work were initiated while Boris Dewitte was at CIMOBP (modelling centre at IMARPE, Peru). Katerina Goubanova was supported by CNES (Centre National d'Etudes Spatiales, France). Jorge Vazquez-Cuervo was supported under contract with the National Aeronautics and Space Administration. We would like to thank the Peru–Chile Climate Change (PCCC) program of the Agence Nationale de la Recherche (ANR) for financial support. This work was performed using HPC resources from CALMIP (Grant 2011-[1044]). We are grateful to Dr. Ben Giese from Texas A&M University for providing the SODA data. Pr. D. Gushchina (University of Moscow) is also acknowledged for fruitful discussions on a previous version of this manuscript.

References

Adler, R.F., Huffman, G.J., Chang, A., Ferraro, R., Xie, P.P., Janowiak, J., Rudolf, B., Schneider, U., Curtis, S., Bolvin, D., Gruber, A., Susskind, J., Arkin, P., Nelkin, E., 2003. The Version 2 Global Precipitation Climatology Project (GPCP) monthly precipitation analysis (1979–present). J. Hydrometeorol. 4, 1147–1167.

Ashok, K., Behera, S.K., Rao, S.A., Weng, H., Yamagata, T., 2007. El Niño Modoki and its possible teleconnection. J. Geophys. Res. 112, C11007, http://dx.doi.org/10.1029/2006JC003798.

Bakun, A., 1990. Global climate change and intensification of coastal ocean upwelling. Science 247, 198–201.

Bakun, A., Weeks, 2008. The marine ecosystem off Peru: what are the secrets of its fishery productivity and what might its future hold? Prog. Oceanogr. 79, 290–299.

Belmadani, A., Echevin, V., Dewitte, B., Colas, F. 2012. Equatorially forced intraseasonal propagations along the Peru–Chile coast and their relation with the nearshore eddy activity in 1992–2000: a modelling study. J. Geophys. Res.-Oceans 117, C04025, http://dx.doi.org/10.1029/2011JC007848.

Björnsson, H., Venegas, S.A., 1997. A Manual for EOF and SVD Analyses of Climatic Data. CCGCR Report no. 97-1. McGill University, Montréal, Québec, 52 pp.

Carton, J.A., Chepurin, G., Cao, X., 2000. A simple ocean data assimilation analysis of the global upper ocean 1950–95. Part I: methodology. J. Phys. Oceanogr. 30, 294–309.

Carton, J.A., Giese, B.S., 2008. A reanalysis of ocean climate using Simple Ocean Data Assimilation (SODA). Mon. Weather Rev. 136 (8), 2999–3017.

Clarke, Allan J., Van Gorder, Stephen, 1994. On ENSO coastal currents and sea levels. J. Phys. Oceanogr. 24, 661–680.

Chelton, D.B., Schlax, M.G., Freilich, M.H., Milliff, R.F., 2004. Satellite measurements reveal persistent small-scale features in ocean winds. Science 303, 978–983, http://dx.doi.org/10.1126/science.1091901.

daSilva A., Young, A.C., Levitus, S. 1994. Atlas of surface marine data 1994. Algorithms and procedures. vol. 1 Technical Report 6, US Department of Commerce, NOAA, NESDIS.

Dewitte, B., Purca, S., Illig, S., Renault, L., Giese, B., 2008. Low frequency modulation of the intraseasonal equatorial Kelvin wave activity in the Pacific ocean from SODA: 1958–2001. J. Clim. 21, 6060–6069.

Dewitte, B., Choi, J., An, S.-I., Thual, S., 2011a. Vertical structure variability and equatorial waves during Central Pacific and Eastern Pacific El Niño in a coupled general circulation model. Clim. Dyn. http://dx.doi.org/10.1007/s00382-011-1215-x.

Dewitte, B., Illig, S., Renault, L., Goubanova, K., Takahashi, K., Gushchina, D., Mosquera, K., Purca, S., 2011b. Modes of covariability between sea surface temperature and wind stress intraseasonal anomalies along the coast of Peru from satellite observations (2000–2008). J. Geophys. Res. 116, C04028, http://dx.doi.org/10.1029/2010JC006495.

Dewitte, B., Reverdin, G., Maes, C., 1999. Vertical structure of an OGCM simulation of the equatorial Pacific Ocean in 1985–1994. J. Phys. Oceanogr. 29, 1542–1570.

Donlon, C., Robinson, I., Casey, K.S., Vazquez-Cuervo, J., Armstrong, E., Arino, O., Gentemann, C., May, D., Le Borgne, P., Piolle, J., Barton, I., Beggs, H., Poulter, D.J.S., Merchant, C.J., Bingham, A., Heinz, S., Harris, A., Wick, G., Emery, B., Minnett, P., Evans, R., Llewellyn-Jones, D., Mutlow, C., Reynolds, R.W., Kawamura, H., Rayner, N., 2007. The global ocean data assimilation experiment high-resolution sea surface temperature pilot project. Bull. Am. Meteorol. Soc. 88, 1197–1213.

Dukowicz, J., Smith, R.D., 1994. Implicit free-surface method for the Bryan–Cox–Semtner ocean model. J. Geophys. Res. 99, 7991–8014.

Efron, B., 1982. The Jackknife, the Bootstrap, and Other Resampling Plans, vol. 38. Society for Industrial and Applied Mathematics CBMSNSF Monographs (pp. 1–92).

Flores, R., Tenorio, J., Dominguez, N., 2009. Variaciones de la extensión Sur de la Corriente Cromwell frente al Perú entre los 3–14°S. Boletín Instituto del Mar del Perú 24 (1–2), 45–55 (in Spanish).

Goubanova, K., Echevin, V., Dewitte, B., Codron, F., Takahashi, K., Terray, P., Vrac, M., 2011. Statistical downscaling of sea-surface wind over the Peru–Chile upwelling region: diagnosing the impact of climate change from the IPSL-CM4 model. Clim. Dyn. http://dx.doi.org/10.1007/s00382-010-0824-0.

Gutierrez, D., Enriquez, E., Purca, S., Quipuzcoa, L., Marquina, R., Flores, G., Graco, M., 2008. Oxygenation episodes on the continental shelf of central Peru: remote forcing and benthic ecosystem response. Prog. Oceanogr. 79, 177–189.

Gutierrez, D., Bouloubassi, I., Sifeddine, A., Purca, S., Goubanova, K., Graco, M., Field, D., Mejanelle, L., Velazco, F., Lorre, A., Salvatteci, R., Quispe, D., Vargas, G., Dewitte, B., Ortlieb, L., 2011a. Coastal cooling and increased productivity in the main upwelling zone off Peru since the mid-twentieth century. Geophys. Res. Lett. 38, L07603, http://dx.doi.org/10.1029/2010GL046324.

Gutiérrez, D., Bertrand, A., Wosnitza-Mendo, C., Dewitte, B., Purca, S., Peña, C., Chaigneau, A., Tam, J., Graco, M., Echevin, V., Grados, C., Fréon, P., Guevara-Carrasco, R., 2011b. Sensibilidad del sistema de afloramiento costero del Perú al cambio climático e implicancias ecológicas. Rev. Peru. Geo-Atmosferia RPGA 3, 1–26. (in Spanish).

Hendon, H.H., Wheeler, M.C., Zhang, C., 2007. Seasonal dependence of the MJO–ENSO relationship. J. Clim. 20, 531–543.

Huyer, A., Knoll, M., Paluzkiewicz, T., Smith, R.L., 1991. The Peru undercurrent: a study in variability. Deep-Sea Res. 39, 247–279.

Jin, F.-F., 1997. An equatorial ocean recharge paradigm for ENSO. Part I: conceptual model. J. Atmos. Sci. 54, 811–829.

Jones, C., Carvalho, L.M.V., 2006. Changes in the activity of the Madden–Julian oscillation during 1958–2004. J. Clim. 19, 6353–6370.

Kao, H.-Y., Yu, J.-Y., 2009. Contrasting Eastern-Pacific and Central-Pacific types of ENSO. J. Clim. 22, 615–632.

Kalnay, E., et al., 1996. The NCEP/NCAR 40-year reanalysis project. Bull. Am. Meteorol. Soc. 77 (3), 437–471.

Kilpatrick, K.A., Podesta, G.P., Evans, R., 2001. Overview of the NOAA/NASA Pathfinder algorithm for sea surface temperature and associated matchup database. J. Geophys. Res. 106, 9179–9197.

Kug, J.-S., Choi, J., An, S.-I., Jin, F.-F., Wittenberg, A.-T., 2010. Warm pool and cold tongue el nino events as simulated by the GFDL2.1 coupled GCM. J. Climate 23, 1226–1239.

Kug, J.-S., Jin, F.-F., An, S.-I., 2009. Two types of El Niño events: cold tongue El Niño and warm pool El Niño. J. Clim. 22, 1499–1515.

Large, W., McWilliams, J., Doney, S., 1994. Oceanic vertical mixing: a review and a model with a nonlocal boundary layer parameterization. Rev. Geophys. 32, 363–403.

Larkin, N.K., Harrison, D.E., 2005. Global seasonal temperature and precipitation anomalies during El Niño autumn and winter. Geophys. Res. Lett. 32, L13705, http://dx.doi.org/10.1029/2005GL022738.

Lee, T., McPhaden, M., 2010. Increasing intensity of El Nino in the central-equatorial Pacific. Geophys. Res. Lett. 37, L14603, http://dx.doi.org/10.1029/2010GL044007.

McPhaden, M.J., Busalacchi, A.J., Cheney, R., Donguy, J.R., Gage, K.S., Halpern, D., Ji, M., Julian, P., Meyers, G., Mitchum, G.T., Niiler, P.P., Picaut, J., Reynolds, R.W., Smith, N., Takeuchi, K., 1998. The Tropical Ocean-Global Atmosphere (TOGA) observing system: a decade of progress. J. Geophys. Res. 103, 14,169–14,240.

Marchesiello, P., Estrade, P., 2010. Upwelling limitation by geostrophic onshore flow. J. Mar. Res. 68, 37–62.

Marchesiello, P., McWilliams, J., Shchepetkin, A., 2001. Open boundary conditions for long-term integration of regional oceanic models. Ocean Model. 3, 1–20.

Marchesiello, P., McWilliams, J., Shchepetkin, A., 2003. Equilibrium structure and dynamics of the California current system. J. Phys. Oceanogr. 33, 753–783.

Please cite this article as: Dewitte, B., et al., Change in El Niño flavours over 1958–2008: Implications for the long-term trend of the upwelling off Peru. Deep-Sea Res. II (2012), http://dx.doi.org/10.1016/j.dsr2.2012.04.011

ARTICLE IN PRESS

Montes, I., Colas, F., Capet, X., Schneider, W., 2010. On the pathways of the equatorial subsurface currents in the eastern equatorial Pacific and their contributions to the Peru–Chile Undercurrent. J. Geophys. Res. 115, C09003, http://dx.doi.org/10.1029/2009JC005710.

Penven, P., Echevin, V., Pasapera, J., Colas, F., Tam, J., 2005. Average circulation, seasonal cycle, and mesoscale dynamics of the Peru Current System: a modeling approach. J. Geophys. Res. 110, C10021, http://dx.doi.org/10.1029/2005JC002945.

Pizarro, O., Clarke, A.J., Van Gorder, S., 2001. El Niño sea level and currents along the South American coast: comparison of observations with theory. J. Phys. Oceanogr. 31 (7), 1891–1903.

Pizarro, O., Shaffer, G., Dewitte, B., Ramos, M., 2002. Dynamics of seasonal and interannual variability of the Peru–Chile Undercurrent. Geophys. Res. Lett. 29 (12). (Art. no. 1581).

Rayner, N.A., Parker, D.E., Horton, E.B., Folland, C.K., Alexander, L.V., Rowell, D.P., Kent, E.C., Kaplan, A., 2003. Global analyses of sea surface temperature, sea ice, and night marine air temperature since the late nineteenth century. J. Geophys. Res. 108 (D14), 4407, http://dx.doi.org/10.1029/2002JD002670.

Reynolds, R., Smith, T.M., 1994. Improved global sea surface temperature analyses using optimum interpolation. J. Clim. 7, 929–948.

Reynolds, et al., 2002. An improved in situ and satellite SST analysis for climate. J. Clim. 15, 1609–1625.

Reynolds, R.W., Chelton, D.B., 2010. Comparisons of daily sea surface temperature analyses for 2007–08. J. Clim. 23, 3545–3562.

Roundy, P.E., Kravitz, J.R., 2009. The association of the evolution of intraseasonal oscillations to ENSO phase. J. Clim. 22, 381–395.

Shchepetkin, A.F., McWilliams, J.C., 2005. The regional oceanic modeling system: a split-explicit, free-surface, topography-following-coordinate ocean model. Ocean Model. 9, 347–404.

Skamarock, W.C., Klemp, J.B., Dudhia, J., Gill, D.O., Barker, D.M., Wang, W., Powers, J.G., 2005. A Description of the Advanced Research WRF Version 2. NCAR Technical note NCAR/TN-468+STR.

Smith, R.D., Dukowicz, J.K., Malone, R.C., 1992. Parallel ocean general circulation modeling. Physica D 60, 38–61.

Takahashi, K., Montecinos, A., Goubanova, K., Dewitte, B., 2011. ENSO regimes: reinterpreting the canonical and Modoki El Niño. Geophys. Res. Lett. 38, L10704, http://dx.doi.org/10.1029/2011GL047364.

Taylor, K.E., 2001. Summarizing multiple aspects of model performance in a single diagram. J. Geophys. Res. 106, 7183–7192.

Uppala, S.M., et al., 2005. The ERA40 reanalysis. Q. J. R. Meteorol. Soc. 131, 2961–3012.

Vázquez-Cuervo, J., Armstrong, E.M., Casey, K.S., Evans, R., Kilpatrick, K., 2010. Comparison between the Pathfinder versions 5.0 and 4.1 sea surface temperature datasets: a case study for high resolution. J. Clim. 23, 1047–1059.

Weng, H., Ashok, K., Behera, S.K., Rao, S.A., Yamagata, T., T., 2007. Impacts of recent El Niño Modoki on dry/wet conditions in the Pacific Rim during boreal summer. Clim. Dyn. 29, 113–129.

Weng, H., Behera, S.K., Yamagata, T., 2009. Anomalous winter climate conditions in the Pacific Rim during recent El Niño Modoki and El Niño events. Clim. Dyn. 32, 663–674.

Yeh, S.-W., Kug, S.-J., Dewitte, B., Kwon, M.-H., Kirtman, B.P., Jin, F.-F., 2009. El Niño in a changing climate. Nature 461, 511–514.

Yu, J.-Y., Kim, S.T., 2011. Relationships between extratropical sea level pressure variations and the Central Pacific and Eastern Pacific types of ENSO. J. Clim. 24, 708–720.

Yu, J.-Y., Kao, H.-Y., Lee, T., 2010. Subtropics-related interannual sea surface temperature variability in the central equatorial Pacific. J. Clim. 23, 2869–2884.

Yu, J.-Y., Kim, S.T., 2010. Three evolution patterns of Central-Pacific El Niño. Geophys. Res. Lett. 37, L08706, http://dx.doi.org/10.1029/2010GL042810.

Please cite this article as: Dewitte, B., et al., Change in El Niño flavours over 1958–2008: Implications for the long-term trend of the upwelling off Peru. Deep-Sea Res. II (2012), http://dx.doi.org/10.1016/j.dsr2.2012.04.011